The Sacrificial Protection of Steel by Zinc-Containing Sol-Gel Coatings

N. Wint,[1,*,z] S. L. Wijesinghe,[2] W. Yan,[2] W. K. Ong,[2] L. Y. Wu,[2] G. Williams,[1] and H. N. McMurray[1,*]

[1]Materials Research Centre, College of Engineering, Swansea University, Bay Campus, Swansea SA1 8EN, United Kingdom

[2] Singapore Institute of Manufacturing Technology (SIMTech), Agency for Science Technology and Research (A* STAR), Singapore 138634

*Electrochemical Society Member.

[z]E-mail: n.wint@swansea.ac.uk

Abstract:

The scanning vibrating electrode technique (SVET), electrochemical impedance spectroscopy, and salt spray testing are used to investigate the ability of Zn rich sol-gel coatings to provide sacrificial protection to carbon steel. Three types of coatings (containing either Zn powder, a coloured pigment, or both) are applied to steel. Intact coatings are shown to act as barrier layers through which electrolyte ingresses over time. Under conditions where the substrate is exposed by an artificial coating defect, SVET is used to investigate the extent to which different coatings offer sacrificial protection when the defect size is systematically changed. The total anodic current, as derived using SVET, doubles when the defect covers 25 % of the total area compared to when 12 % of the area is exposed. This finding is consistent with efficient sacrificial protection of the steel by the zinc based coating. This sacrificial protection is observed for up to 24 hours for cases

where the defect constitutes up to 52 % of total area. The protection offered in the presence of a coloured pigment is delayed and it is proposed that the pigment restricts the ability of Zn to couple with the underlying steel.

1. Introduction

The use of sol-gel coatings to provide corrosion protection has been a topic of interest for the last few decades, [1] and has been stimulated by the ongoing need for environmentally friendly and non-toxic alternatives to chromate conversion coatings and pre-treatments. [2-4] Research has been focused on the use of sol-gel coatings as adhesion promoters when applied between a metal substrate and an organic primer/topcoat. [5-6] Their ability to provide effective corrosion protection has also been investigated on technologically important metals such as Cu, [7-8] Al [7,9] alloys, Mg [10] and carbon steel. [11]

The production of sol-gel coatings occurs at low temperatures at which thermal degradation and volatilization is minimised. The use of liquid alkoxysilane precursors also means that sol gel technology can be used to over-coat surfaces of complex shapes. [12] Hydrolysis (Equation 1), and subsequent condensation (Equation 2) results in the production of silanol groups and siloxane bonds respectively. As the polymer structures agglomerate, networks extend into the liquid phase causing thickening and the production of a gel. [12]

$$R - Si(OR)_3 \leftrightarrow R - Si(OH)_3 \quad (1)$$

$$-Si - OH + HO - Si - \leftrightarrow -Si - O - Si - + H_2O \quad (2)$$

Shrinkage occurs during the subsequent drying stage and the resultant coating can be brittle for thicknesses > 100 μm. [13] At lower thickness values, porosity increases and the performance is compromised. Research efforts have subsequently focused on the

production of hybrid sol-gel derived coatings which encompass the properties of both organic polymeric materials and inorganic/ceramic constituents. [14]

However, sol-gel coatings are only able to provide barrier protection to the steel substrate and are unable to provide active corrosion protection in the case that a large area of the coating is breached. Several pieces of work have focused on the application of hybrid sol-gel coatings, some of which have been doped with corrosion inhibitors, to hot dipped zinc galvanized (HDG). [15-17] Zn is more anodically active than steel and is therefore able to provide cathodic protection to the substrate (in addition to the barrier protection offered by the sol-gel). However, galvanizing primarily takes place via a hot dipping process whereby steel components/structures are submerged within a molten bath of the coating metal. This process cannot be completed at the point of use and is therefore associated with substantial economic costs. One alternative to hot dip galvanising is the application of Zn rich coatings, which consist of Zn particles dispersed in a binder. Such systems are available in a liquid form and can be applied to steel substrates as a paint.

Addition of Zn particles or flakes can be made to both organic or inorganic binders and Zn-rich primers have been made in this way for use on various steels. [18-30] Only Zn particles which are in electrical contact with the steel substrate are able to contribute to the sacrificial protection offered by such coatings, and the critical volume fraction must therefore be higher than the percolation threshold. [18-19] When the electrolyte reaches the steel/coating interface the active Zn provides cathodic protection to the underlying substrate for a period of time. Zn dissolution results in the loss of contact with the steel, after which, corrosion product can form and eventually prevents galvanic coupling. [18, 22] At longer time periods the corrosion product must seal the pores to ensure adequate protection. [20-22] Basic Zn salts, deposited at the substrate, have also been suggested to act

as corrosion inhibitors. [29-32] The ability of Zn sol-gel coatings to act sacrificially to a steel substrate means that they are considered as suitable alternatives to HDG, especially for cases where production levels and capital investment are low.

The chemical stability and enhanced oxidation and corrosion resistance afforded by sol-gel coatings [12] also makes them viable candidates for coating of the advanced high strength steel (AHSS) and ultra-high strength steel (UHSS) grades increasingly used for automotive applications. To achieve the desired mechanical properties, steel parts are press hardened at temperatures of up to 950 °C. [33] The oxidation resistance of components is therefore of importance to avoid detrimental changes to both mechanical properties and surface appearance. Thin, sol-gel coatings have previously been applied to the boron-manganese steel alloy 22MnB5 with the aim of improving oxidation resistance. [33] The coatings were found to protect against oxidation up to 800°C and remained intact during press hardening. [33] The absence of secondary phase intermetallics and residues (which can form during the subsequent laser beam welding process) highlights the suitability of sol-gel coatings to further industrial processing. [33] The corrosion properties of 'higher abrasion resistant' sol-gel Zn-SiO_2 thin films have previously been characterized using electrochemical impedance spectroscopy (EIS). [34] The films were shown to behave differently to conventional sacrificial Zn based coatings (such as HDG), and any enhanced corrosion protection was proposed to be a result the tendency of Zn to react with Cl^- ions to form $ZnCl_2$ and meant that the coatings were deemed suitable for use in marine environments. The question of whether Zn sol-gel coatings are able to provide sacrificial protection to a steel substrate therefore remains largely unanswered. [34]

The success of an active coating can be characterised by the distance over which the system is able to protect a coating defect (throwing power), as well as the time before

coating failure. The barrier properties of the 'binder' material, alongside the anode/cathode area ratio and geometry also play a role in influencing the galvanic protection offered by such coatings. In the work described in this paper we make use of an in situ scanning vibrating electrode technique (SVET) to study the ability of Zn rich sol-gel composite coatings to provide sacrificial protection to steel. For active coatings, the position and intensity of the net anodic and cathodic regions change with respect to time. The spatial and temporal resolution of corrosion current density offered by the SVET therefore provides advantages over conventional electrochemical techniques and the technique has previously been used to analyse the ability of an Mg rich primer to become the net anode in a Mg rich primer/ defect galvanic couple formed on unpolarised AA2024-T3. [35] The aim of the present work is to semi-quantitatively assess the ability of Zn sol-gel coatings to provide sacrificial protection to a steel substrate. As such, the size of the defect is systematically changed and the total integrated anodic and cathodic current density values associated with the defined regions, are calculated. Consumer driven aesthetical requirements, especially in urban areas such as Singapore, have led to the application of multiple layers which introduce colour into the system. Intermediate layers enhance adhesion and layer compatibility, but result in greater economic costs and overall corrosion resistance. The sacrificial protection afforded by coloured coatings, is therefore compared to that provided by their uncoloured counterparts.

2. Experimental

2.1 Coating Manufacture

A sol-gel based binder was manufactured using a methodology described previously and shown in Figure 1. [36] Briefly, Tetraethyl orthosilicate (TEOS, Sigma Aldrich) was used

as an alkoxysilane precursor. TEOS and (3-Glycidyloxypropyl) trimethoxysilane (GLYMO, Sigma Aldrich) were mixed with molar ratio 3:2, and hydrolyzed in 0.5 M itaconic acid (≥99 %, Sigma Aldrich) solution, with the presence of 5 wt.% LUDOX® AS-40 colloidal silica (Sigma Aldrich). The mixture was stirred at 500 rpm for 72 to 120 hours to ensure complete hydrolysis before ageing. Basic coating additives (released during curing) and Zn powder (>98 % purity) were added and the mixture was mechanically stirred for 10 minutes. A spray coating technique was used to apply the coating to SA2.5 sand blasted (ISO 8501-1) A36 carbon steel. [37] The nominal chemical composition of ASTM A36 is; carbon 0.25 - 0.29 %, copper 0.2%, manganese 0.8 – 1.2%, phosphorous 0.04 %, silicon 0.15 -0.40%, sulfur 0.04% and the iron(balance). Curing took place at 150 °C for 30 minutes.

(Figure 1)

In the case of coloured samples, a colouring blend was prepared by ball milling a phthalocyanine based colourant (Heliogen Green L8605, BASF) to ~300 nm and dispersing within ethanol. This colourant is widely used throughout the coating industry and is highly stable and associated with desirable lightfastness properties. [38] The colouring blend was added to sol-gel together with coating additives and Zn powder. Three different coatings were investigated during this work; a coloured sol-gel coating (CSG), a Zn rich sol-gel coating (ZnSG) and a coloured Zn rich sol-gel coating (CZnSG). The thickness and composition of the dry coatings are shown in Table 1. It should be borne in mind that the amount of Zn incorporated into the coatings is ~ 60 % (by volume) and less than than typically used (~ 80 Vol. %) [21, 23, 28] It has previously been shown that zinc rich coatings provide corrosion protection to steel for longer periods of time at increased values of concentration. [39]

(Table 1)

The coatings used throughout the work described in this paper are therefore composite materials which can be physically, and electrically, represented by either three or four components (given in the Table 1). All coatings comprise an electrically insulating matrix, within which clusters of interconnecting pores exist. These pores can become filled with electrolyte and may therefore exhibit ionic conductivity after periods of immersion. ZnSG coatings contain clusters of electonically conducting Zn particles which are linked ohmically. Green coloured pigments are also included in CSG and CZnSG coatings.

2.2 Resistivity measurements

Sheet resistance measurements were made using a CDE ResMAP 178 resistivity monitor and then converted to conductivity. At least three readings were taken in each case.

2.3 Adhesion Measurements

Adhesion of the ZnSG and CZnSG coatings to the carbon steel substrates was assessed by applying and removing pressure sensitive tape over cuts made in the coating according to the test method specified by ASTM D3359 (Measuring Adhesion by Tape Test). [40]

2.4 Salt Spray

Both scribed and unscribed coated coupons were exposed to an accelerated cyclic corrosion test according to ISO 14993 (intermittent wet and dry conditions) to evaluate the corrosion protective performance. [41] For each test, three pieces of sample were exposed as triplicates and representative images are shown.

2.5 Open circuit potential

A Solartron 1287 potentiostat was used to record the free corrosion potential (E_{corr}) values associated with intact coatings immersed in 0.86 M NaCl for 24 hours. A saturated calomel reference electrode was used and. Three measurements were made for each sample and representative data are shown.

2.6 EIS

Electrochemical impedance spectroscopy (EIS) was used to investigate the through pore ionic conductivity of the coatings. EIS experiments were carried out using a Solartron 1287 electrochemical interface coupled with a 1255 frequency response analyzer. A standard three-electrode cell was employed and incorporated a SG coated steel sample coupon working electrode, a platinum gauze counter electrode and a saturated calomel reference electrode. The input AC amplitude was 10 mV and the frequency range was from 0.05 Hz to 100 kHz. Impedance spectra were obtained at 1 hour intervals. Two measurements were made for each coating and representative data are shown.

2.7 SVET

Extruded PTFE tape (type 5490 HD supplied by 3 M) was used to expose a 9 mm x 9 mm area in the centre of each coupon. Defects in the coating were created by mechanical abrasion using a scalpel blade.

SVET is used to study aqueous corrosion and makes use of the ionic current flux that exists in the electrolyte above a corroding sample. The inherent resistance of the electrolyte results in the presence of an ohmically generated potential field. [42-45] The vibrating SVET microtip is able to sense an alternating potential at its vibration frequency. The value detected by the SVET is then proportional to the potential gradient (or electric field strength) in the direction of vibration and thus to the current.[42-46]

The SVET apparatus has been described in detail previously. [43] The SVET microtip is comprised of a platinum microelectrode (125 µm) which is sealed in by a glass sheath and has a total diameter of 250 µm. The probe was vibrated, via a pushrod, at a frequency of 140 Hz using an electromagnetic driver. The probe vibration amplitude was 25 µm. µ metal was used to enclose the electromagnetic driver and minimise electromagnetic flux leakage. The wiring and pushrod were surrounded by an aluminium cylinder. Vibration of the tip was constrained to the perpendicular direction by use of a bearing. A 2.5 cm x 2.5 cm chloridized low impedance silver chloride reference electrode was attached to the cylinder at a distance of ca. 5 cm away from the probe.

Three stepper motors (Time and Precision Ltd) were used to move the SVET probe and a Perkin Elmer 7265 lock-in amplifier was used to detect a SVET voltage signal. Measurements of the peak-to-peak SVET probe vibration amplitude (a_{pp} = 30 +/- 5 µm) were conducted in air using a stroboscope, in combination with a travelling microscope.

Ohm's law $V_{pp} = j_z (a_{pp}/K)$ can be used to relate the peak-to-peak SVET voltage signal V_{pp} to the current flux density measured along the axis of probe vibration normal to the sample surface (j_z). and the quantity a_{pp}/K is defined as the SVET calibration factor. [42-46] A specially constructed two-compartment calibration cell was used. One of the compartments consisted of a nylon beaker and contained a 1 cm^2 platinum electrode. The other compartment was a 6 dm^3 tank which contained the experimental electrolyte. A 1 cm^2 platinum electrode was also present in the second compartment. Both silver chloride electrodes were immersed within the electrolyte and the intra-electrode spacing was 10 – 20 cm. The compartments were connected by a 6 cm long, vertically orientated 0.5 cm diameter tube. The SVET microtip was positioned in the tube and the current flux density was assumed to be constant across the tube diameter meaning that current flux aligned

vertically (in a direction which was parallel with both the axis of the tube and the direction of tip vibration). A battery powered galvanostat was used to pass currents (of known value) through the tube. The SVET V_{pp} signal generated was recorded and a calibration factor was calculated using the generated plots. This factor allowed SVET V_{pp} signals to be converted to j_z values.

Following calibration, samples were securely attached to the bottom of the SVET tank. Scans were conducted immediately following immersion in 0.86 M NaCl, and every 30 minutes thereafter for a 24-hour period. The SVET probe was scanned perpendicular to the surface of the sample and the probe-sample spacing was 100 μm. The electrolyte was unstirred at a temperature of 20 °C.

Only the localized corrosion currents which arise from anodic and cathodic sites separated by distances greater than the scan height (in this case 100 μm) can be efficiently detected by SVET. For cases when the spacing is smaller than the scan height, the current flux lines will no longer cross the plane of scan and will not be detected (or at best inefficiently). [42, 46] The SVET response peak for a point current source has a theoretical width at half maximum (*whm*) of 1.53*z* (where *z* is the probe height). [47-48] The electrically sensitive part of the micro-tip has a finite width and peak broadening occurs. The *whm* for the SVET used here has previously been listed as ~ 260 μm when *z*=100 μm.[46]

Surfer 8 (Golden Software) was used to plot SVET derived j_z data. Positive j_z values were numerically integrated (via Equation 3) to obtain both the total anodic current ($I_{a(t)}$) and area-averaged total anodic current density ($J_{a(t)}$) associated with each scan.

$$I_{at} = A.J_{a(t)} = \int_0^X \int_0^Y [\, j_{z(x,y,t)} > 0]\, dx\, dy \qquad (3)$$

where X and Y are the scan dimensions and A is the scan area. Similarly, negative j_z values can be used to obtain total cathodic current ($I_{c(t)}$) and area-averaged total cathodic current density ($J_{c(t)}$).

Faraday's law (Equation 4) can then be used to calculate the total amount of charge density and mass loss associated with local anodes over the entire experimental time period

$$q = \frac{2Fm}{M} = \int_{t=0}^{t=t_{max}} j_t \mathrm{d}t \quad (4)$$

where q is the total charge density, m is the mass loss per unit area, M is the atomic weight of Zn (65.38 Da), n is the valence of metal ions (2), F is the Faraday constant, t_{max} is the total immersion time. In all cases it is assumed that i_t remained constant between scans.

3. Results

3.1 Resistivity measurements

The conductivity values associated with each type of coating are shown in Table 2. Data intervals correspond to one standard deviation on the mean of three measurements. In the absence of Zn, the conductivity of the coating was less than the lowest quantity which could be measured by the available instrumentation. In comparison, a value of 250 $S.m^{-1}$ was obtained for ZnSG coatings, this falling to 170 $S.m^{-1}$ in the case of CZnSG.

(Table 2)

3.2 Adhesion Measurements

A rating of 5B (0 % coating removed) was recorded for ZnSG. Results for CZnSG varied between 4B (less than 5% of the coating removed) and 3B (5% to 15% of the coating removed).

3.3 Salt spray

The capability of coatings to provide corrosion protection to the steel substrate was evaluated using accelerated corrosion exposure testing. During the 42 day period of exposure, the coated samples were removed from the accelerated corrosion test chamber for periodical evaluation. Photographs of the sample type after each time period are shown in Figures 2-4.

The appearance of the CSG coating at various time intervals is shown in Figure 2. In the case of unscribed samples (Figure 2a), brown Fe based corrosion product can be seen on the sample surface within a few days and is assumed to form at defects in the coating, or where the electrolyte has percolated through the coating. In the case of the scribed sample (Figure 2b), red rust can be observed almost immediately and covers the entire surface after 7 days.

Whilst the amount of white Zn corrosion product on ZnSG coatings increases with time (Figure 3), substrate corrosion is not observed on un scribed (Figure 3a) or scribed (Figure 3b) samples for the entire 42 day exposure period.

The appearance of the CZnSG coating at various time intervals is shown in Figure 4. The corrosion protection capability (specially the sacrificial corrosion protection) is clearly retained in the presence of coloured pigments. However, after several days of exposure in the accelerated chamber, the formation of Zn corrosion products changes the aesthetics of the coupons.

(Figure 2)

(Figure 3)

(Figure 4)

3.4 OCP Results

Figure 5 shows the free corrosion potential (E_{corr}) of coated steel samples, immersed in 0.86 M NaCl, as a function of immersion time. The E_{corr} measured for the A36 steel substrate is ~0.45 V vs. SHE, and consistent with that expected for freely corroding steel. In the case of CSG coatings (in the absence of Zn particles), E_{corr} is in the range of -0.4 vs. SHE, which indicates no cathodic protection[49-52] at all times and is similar to that recorded for the bare steel substrate. For ZnSG and CZnSG coatings, E_{corr} remains below -0.76 V vs. SHE for the 24 hour time period indicating cathodic protection of the substrate. [49-52] Figure 5 also shows that E_{corr} values for both ZnSG coatings increase approximately linearly with time after immersion, which is indicative of the gradual dissolution of Zn.

(Figure 5)

3.5 EIS Results

Figure 6 shows the Bode plots obtained for a.) CSG and b.) CZnSG obtained after immersion in 0.86 M NaCl for varying periods of time and Table 3 shows time dependent low frequency impedance values obtained from Figure 6. For CSG coatings, the value of $|Z|$ remains fairly uniform over the frequency range and decreases with immersion time. The phase angle remains near zero (~-10 °) for the entire time of immersion (Figure 6a).

For CZnSG coatings, the values of $|Z|$ recorded (Figure 6b) are ~3 times smaller than those measured in the absence of Zn. The gradient of the $|Z|$ Bode plot tends toward -0.5 (Figure 6b) after longer periods of immersion. The phase angle values recorded at the lowest frequencies during the initial times of immersion indicate that the overall circuit impedance is dominated by resistive elements. The same is true at the high frequency limit at which $|Z|$ tends toward the solution resistance ($R_{solution}$). The deviation away from this behaviour at longer immersion times (20-24 hours) is likely to be a result of the system becoming diffusion limited.

(Figure 6)

(Table 3)

3.6 SVET Results

Intact coatings: Figure 7 shows the SVET derived normal current density values measured above CSG, ZnSG and CZnSG coatings immersed in 0.86 NaCl after various periods of time. For CSG coatings (Figure 7a) the anodic (red) and cathodic (blue) j_z values recorded are relatively small and spread evenly over the surface of the sample. The j_z values recorded above ZnSG coated steel (Figure 7b) are an order of magnitude larger than those observed for CSG coatings and in the region of those expected in the case that electron transfer is not limited by an insulating coating. The cathodic current is spread evenly across the surface and appears to dominate the sample surface. This effect has previously been attributed to the vibration of the SVET probe which tends to increase the transport of O_2 to the metal surface [53-54] and which has previously been shown to increase the oxygen reduction current by 3-4 times.[53] It is also worth considering that SVET detects net current values and is only able to detect localized corrosion currents which

arise from anodic and cathodic sites separated by distances greater than the scan height (in this case 100 μm). In the case of general corrosion the current flux lines will no longer cross the plane of scan and will not be detected. [42, 46] It is therefore possible that the SVET is unable to resolve anodic areas present within the 'net' cathodic defect region

Small regions of localized anodic activity are also apparent. The ZnSG coatings are porous and are therefore expected to become permeable with respect to the experimental electrolyte, to some extent at least. However, red rust (indicative of anodic iron dissolution) was not observed anywhere on the sample surface, even at the end of the 24 hour experimental time period. It therefore seems reasonable to assume that the anodic current density regions detected by SVET arise from the sacrificial anodic dissolution of zinc particles in the coating, and not from attack on the underlying steel substrate. In the case of CZnSG coated steel slightly smaller current density values (~0.5 times those measured for ZnSG) were recorded (Figure 7c). The net anodic area appears to increase with immersion time. Figure 8a and 8b show that the corresponding integrated anodic current density, and accumulated mass loss, obtained using Equation 3 and Equation 4 respectively, are higher in the case of CZnSG coatings, compared to ZnSG coatings.

(Figure 7)

(Figure 8)

Sacrificial protection by ZnSG: The ability of ZnSG coatings to provide sacrificial protection to the underlying steel substrate was investigated by creating an artificial coating defect by mechanical abrasion of the coating. Figure 9 shows the SVET derived normal current density values measured above CSG, ZnSG and CZnSG coatings in the presence of a 5 mm x 2 mm (12 % of total area) defect. As expected, for CSG (Figure 9a)

343 the coating is unable to offer any sacrificial protection. Immediately after immersion a net
344 cathodic area covers half of the sample, whilst the other half remains anodic. Fairly
345 rapidly a strong net anode is established in the defect region which is covered in red rust
346 following 24 hours of immersion. Lower j_z values are observed on the intact coating,
347 which acts as a partial barrier to electrolyte ingress. In comparison, for ZnSG coatings
348 (Figure 9b) the exposed steel remains cathodic with respect to the ZnSG surface.
349 Whereas the anodic j_z are distributed evenly over the surface of the intact coating, the
350 anodic j_z recorded for CZnSG coatings are localised at the defect edge during the first 4
351 hours of immersion. The anodic current becomes more evenly distributed as immersion
352 time increases. The re-distribution of anodic activity within the first few hours of
353 immersion can be seen more clearly in Figure 10 which shows the j_z values recorded
354 along the dotted lines in Figure 9c at various times of immersion. Values of up to ~ 1.3
355 $A.m^{-2}$ are observed within the defect region during the initial scan. After just 2 hours this
356 value has fallen significantly and any remaining anodic activity (~ 0.3 $A.m^{-2}$) is localized
357 at the defect/coating interface. After 8 hours the anodic current density at the defect/
358 coating boundary is similar to that observed over the remainder of coated region of the
359 sample. Figure 11b shows j_z values recorded along the dotted lines shown in Figure 9c
360 during the later stages of CZnSG immersion. Between 12 and 20 hours the net cathodic
361 current density progressively decreases from ~ 0.4 $A.m^{-2}$ to ~ - 0.2 A. m^{-2} within the
362 defect region and there is some evidence that the same process occurs for ZnSG coatings.
363 When considering Figure 10 it should be bourne in mind that the j_z values shown are only
364 taken from one scan line and resultantly the anodic and cathodic currents do not balance

For both ZnSG and CZnSG coatings the iron surface behaves as a net cathode for the 24 hour duration of the experiment and red rust is not observed on either surface following 24 hours of immersion.

(Figure 9)

(Figure 10)

Figure 11a and Figure 11b show the corresponding integrated anodic current density, and accumulated mass loss, obtained using Equation 3 and Equation 4, respectively. As with Figure 8, the reason for the higher values obtained for CZnSG coatings is, as yet, unknown. Regardless, it is clear, from both Figure 9 and Figure 11, that ZnSG coatings are able to provide sacrificial protection to the underlying substrate in the presence of the green coloured pigment.

(Figure 11)

Having established the ability of ZnSG coatings to provide sacrificial protection to the underlying substrate, the effect of defect area was investigated. Figure 12 shows the SVET derived normal current density values measured above ZnSG coatings in the presence of defects of varying size. In all cases the defect remained cathodic for the entirety of the experiment time period (24 hours). For defects covering 25 % (Figure 13b) and 52 % (Figure 12c) of the total area, small anodic regions are observed within the cathodic defect region towards the end of the experiment. However, red rust was not observed on the surface after 24 hours of immersion, even in the case of the largest defect (covering 52 % of total area). Figure 13a and Figure 13b show the corresponding integrated anodic current density, and accumulated mass loss, obtained using Equation 3 and Equation 4, respectively. In both cases the values recorded increase when the

exposed area increases from 12 % to 25 %. This increase in Zn dissolution is expected in the case of a bigger cathode area. A decrease in both values are observed when the exposed area is increased to ~52 % of the total area.

(Figure 12)

(Figure 13)

4. Discussion

4.1 CSG coatings: In the absence of Zn, CSG coatings provide barrier protection (and not sacrificial protection) to the underlying substrate (Figure 5). This results in the low j_z values recorded above an intact CSG coating immersed in NaCl (Figure 7a). The values of total impedance $|Z|$ recorded upon initial immersion are low compared to those previously reported for sol-gel coated steel (where coating thickness is comparable to, or less, than that used here) [55-57] This suggests that sol-gel (used in isolation) is a poor barrier coating [58] and is consistent with the known inherent porosity associated with this type of coating. [13] The low phase angles shown in Figure 6a indicate that the system is dominated by resistive characteristics. The value of $|Z|$ is likely to tend toward that of the coating resistance ($R_{coating}$), which is believed to originate from columns of electrolyte which form within the porous structure of the organic polymer coating and allow limited contact between the electrode and solution. As $|Z|$ tends to be dominated by, and have characteristics of, the smallest individual impedance it follows that the capacitor impedance be significantly higher than ~ 1000 $\Omega.cm^{-2}$, even at a frequency of 100, 000 Hz. To check the plausibility of this statement the value of the coating capacitance was calculated using Equation 5, where A is the coating area (in this case 1 cm^2), d is the coating thickness (~ 30 μm) and ε_0 is the permittivity of free space. The dielectric

411 constant of the CSG will vary with water content, but is, in the first instance, assumed to
412 be that of silica (~ 3.8) [59-60]. The calculated value (~ 0.1 nF) can be used in Equation 6 to
413 determine the capacitor impedance at a frequency (*f*) of 100, 000 Hz. The value obtained
414 (10^4 $\Omega.m^{-2}$) is an order of magnitude larger than the value of $|Z|$. This finding is
415 consistent with the system for which $|Z|$ is dominated by the resistive characteristics of
416 the coating. There is a slight decrease in the phase angle at the highest frequency which
417 may indicate that the capacitor impedance is becoming more dominant.

418 $$C = \frac{\varepsilon_0 \varepsilon A}{d} \quad (5)$$

419 $$Z = \frac{1}{2\pi f C} \quad (6)$$

420 The time dependent decrease in $|Z|$ (Figure 6a) is consistent with the gradual ingress of
421 electrolyte which, in time, reaches the steel substrate.

422 In the case that the coating is not fully intact, for example at pores in the coating (Figure
423 2a) or at artificial coating defects (Figure 2b) the CSG is unable to offer sacrificial
424 protection and anodic attack initially occurs within the defect (Figure 9a). As time
425 progresses, the electrolyte will ingress through pores in the CSG to the substrate and it is
426 predicted that a net anode and cathode would eventually divide the underlying steel (as is
427 the case on plain steel).

428 *4.2 ZnSG:* ZnSG coatings are able to provide sacrificial protection to the underlying steel
429 substrate (Figure 5) and substrate corrosion was not observed on intact (Figure 3a) or
430 scribed coatings (Figure 3b) after 42 days of salt spray exposure. Coatings were able to
431 provide sacrificial protection to artificial coating defects (where the underlying steel
432 substrate was exposed) which covered up to 52 % of the total sample area for 24 hours of

immersion in 0.86 M NaCl and red rust is not observed following immersion (Figure 12). The delay in the galvanic effect, and in the establishment of discrete anodic and cathodic sites, increases with defect size. A similar time-dependent evolution of galvanic current was observed during a scanning reference electrode technique (SRET) study into the galvanic corrosion processes occurring in the region of coating defects and cut edges on galvanised (Zn) steel [61-62] The build-up of galvanic current probably reflects a time-dependent depassivation of the zinc surface and the establishment of stable sites of anodic zinc (powder) dissolution. The stabilization and lateral spreading of anodic activity occurs as a consequence of local changes in electrolyte composition at anodic sites. An aggressive anolyte (with reduced pH and increased chloride activity) develops through a combination of electro-migration (of Cl^-) and hydrolysis (of Zn^{2+}).[63-64] The galvanic current produces an alkaline catholyte by forcing the ORR onto the iron surface, leading to the evolution of passivity (and suppression of anodic dissolution) on iron. This process is visualized in Figure 9 and Figure 10 which show that the anodic current is initially concentrated at the defect/coating interface. As time progresses Zn dissolution occurs uniformly along the coating and a plateau in current density is observed.

The increase in SVET derived integrated anodic current density (Figure 13a), and accumulated mass loss (Figure 13b) when the exposed area increases from 12 % to 25 % of the total surface area is consistent with an increase in Zn dissolution which is expected in the case of a larger cathode area. Figure 13b also shows that, between 4 and 12 hours, the total anodic current recorded for a 25 % exposed area is ~ 2 x that measured in the case that 12 % of the area is exposed. This indicates that the anodic current is directly proportional to the exposed area and is consistent with efficient sacrificial protection of the steel by the zinc based coating. The total cathodic current emerging from the defect

457 which covered 25 % of the total area was almost double that recorded when 12 % was
458 exposed. This finding implies that the individual cathodic j_z values (measured on the steel
459 defect) are independent of exposed area and supports the notion that the localised
460 corrosion observed is under cathodic control (i.e twice the anodic current is recorded
461 when doubling the defect area). The progressively decreasing current values with time is
462 likely to be a result cathodic deactivation through precipitation which inhibits the ORR
463 occurring on the steel surface. This 'cathodic self-healing' mechanism has been observed
464 previously during the study of cut edge corrosion occurring on Zn galvanised steel sheet.
465 [65-69] The zinc cations (at the anodic sites) interact with the hydroxide ions (produced at
466 cathodic sites) to form zinc based corrosion products on the active cathode. [65-69] This
467 process is controlled by the increase in interfacial pH and the precipitation of white zinc
468 based corrosion product formed on the region of exposed steel (scribe) in Figure 3 and
469 Figure 4 and within the defect area in Figure 9c.

470 This relationship appears to break down for a larger defect size (defects covering 52 % of
471 the total area). Small anodic regions are observed within the cathodic defect region
472 towards the end of the experiment (Figure 12c) and it is assumed that significant anodic
473 activity becomes co-located on the steel. It then seems plausible that subsequent decrease
474 in integrated anodic current density (Figure 13a), and accumulated mass loss (Figure 13b),
475 observed when the exposed area is increased to 52 % of the total area, is a consequence
476 of the limitations of the SVET to resolve localized corrosion. In the case that spacing is
477 smaller than the scan height, it is possible that current flux lines do not cross the plane of
478 scan and that the SVET is unable to resolve anodic areas present within the 'net' cathodic
479 defect region. [42, 46]

4.3 CZnSG; As demonstrated by the open circuit potential measurements shown in Figure 5, CZnSG coatings are able to provide sacrificial protection to the underlying steel substrate and substrate corrosion is not observed on scribed coatings after 42 days of salt spray exposure (Figure 4). Zn corrosion occurs over the entirety of the intact CZnSG coating, which appear white after 24 hours of immersion (Figure 9c). Corrosion product is also found to form within defects in the CZnSG coatings. This corrosion product build up leads to the reduction in cathodic current density observed in Figure 10. The value of CZnSG coating resistance (obtained using data given in Table 1 and Table 2) is low (~1.8 mΩ), and charge transfer resistance (R_{CT}) is thought to dominate at low frequency values. The gradient of the $|Z|$ Bode plot tends toward -0.5 (Figure 6b) after longer periods of immersion. This is consistent with finite diffusion control and a semi-infinite Warburg diffusion characteristic which is believed to be a result of the more torturous route of oxygen diffusion experienced in the presence of this corrosion product. The reasons for the increase in SVET derived anodic j_z values and the associated accumulated mass loss, recorded for CZnSG compared to ZnSG coatings, is unclear. However, given the reduction in conductivity observed for CZnSG coatings (compared to ZnSG coatings), it is plausible that the coloured pigments give some physical obstructions to Zn connectivity. In the presence of an artificial defect emerging anodic current is focused on the defect edges over the first 4 hours of immersion, and becomes more uniformly distributed as immersion time increases. This is consistent with the notion that the coloured pigment, present in CZnSG coatings, acts as a barrier which restricts the ability of the Zn (present within the coating) to couple with the underlying steel substrate. The defect edge presents a low resistance pathway through which the local galvanic cell current can emerge. It is also plausible that increased porosity/defects exist in coloured

coatings due to the presence of the coating additive used to aid in pigment wetting and dispersion.

Despite the decreased protection observed for CZnSG, the sacrificial protection offered is deemed adequate for a single layer Zn rich coating.

5. Conclusions

An electrochemical investigation into the ability of zinc rich sol gel coatings to provide sacrificial protection to steel substrates was conducted to show that;

- For CSG coatings the impedance remains uniform over the frequency range and the coatings behave as resistors. The value of $|Z|$ decreases with immersion time. For CZnSG coatings the gradient of the $|Z|$ Bode plot tends toward -0.5 after longer periods of immersion and is consistent with a semi-infinite Warburg diffusion characteristic which is believed to be a result of the more torturous route of oxygen diffusion experienced in the presence of this corrosion product.
- For intact CSG coatings SVET derived j_z values are relatively small and consistent with those expected in the case that limited electron transfer occurs. CSG coatings are unable to offer any sacrificial protection in the presence of a coating defect.
- For both ZnSG and CZnSG coatings the exposed steel remains cathodic with respect to the coating for the entire 24-hour experimental time period. The SVET derived integrated anodic current density, and accumulated mass loss values obtained are higher for CZnSG coatings, compared to ZnSG coatings.
- ZnSG coatings are able to provide sacrificial protection (remains cathodic) for 24 hours in the presence of defects which cover up to ~ 52 % of the total sample area.

The SVET derived integrated anodic current density and accumulated mass loss values increase when the exposed area increases from 12 % to 25 %.

It is proposed that;

- CSG coatings are only able to provide barrier protection (not sacrificial protection) to the underlying substrate and anodic attack initially occurs locally within any coating defects. As time progresses the electrolyte will ingress through pores in the CSG and corrosive attack will be spread eventually over the substrate surface.
- ZnSG coatings are able to provide sacrificial protection to the underlying steel and an increase in defect size results in the increased dissolution of Zn and at prolonged time periods anodic dissolution of the underlying substrate may occur.
- CZnSG coatings are able to provide sacrificial protection to the underlying steel substrate. However, it is plausible that the presence of coloured pigments physically obstruct Zn connectivity and act as barriers which restricts the ability of the Zn to couple with the underlying steel substrate. Another possibility is that increased porosity/defects exist due to the presence of the coating additive used to aid in pigment wetting and dispersion.

6. Acknowledgments

Authors would like to thanks Building & Construction Authority (BCA), Singapore for the support for this work through the MNDRF DfMA & BIM Grant Call. We thank industrial collaborators; FRP Products Co Pte Ltd and ZINGAMETALL(S) Pte Ltd for their support.

7. Tables

550 Table 1. Coating composition.

	Coloured SG	**ZnSG**	**Coloured ZnSG**
Thickness (µm)	38±5	31±5	30±5
Sol gel (Vol %)	91.5	37.3	36.9
Zinc (Vol %)	0	60.4	59.7
Silica (Vol %)	5.5	2.2	2.2
Green Pigment (Vol %)	3.0	0	1.2

551 Table 2. Coating conductivity Measurements.

	Conductivity ($S.m^{-1}$)
ZnSG	250±47
Coloured ZnSG	170±32
SG	$< 2 \times 10^{-2}$

552 Table 3. EIS derived $|Z|$ at 0.1 Hz.

Immersion time (hours)	$\|Z\|$ ($\Omega.cm^{-2}$)	
	CSG	CZnSG
1	1421	229
2	2822	237
3	1060	221
4	1025	219
5	1015	224
6	995	228
7	991	230
8	978	237
9	977	248
10	972	262
11	961	275
12	853	288
13	845	304
14	842	319
15	748	329
16	735	336
17	732	348
18	730	365
19	730	379
20	727	386
21	730	433
22	720	466
23	715	500
24	712	528

8. Figure Legends

Figure 1. A schematic representation the process followed during the manufacture of the sol-gel based binder.

Figure 2. Optical images of scribed and un scribed CSG coatings after various times of exposure to an accelerated cyclic corrosion test according to ISO 14993.

Figure 3. Optical images of scribed and un scribed ZnSG coatings after various times of exposure to an accelerated cyclic corrosion test according to ISO 14993.

Figure 4. Optical images of scribed and un scribed CZnSG coatings after various times of exposure to an accelerated cyclic corrosion test according to ISO 14993.

Figure 5. E_{corr} as a function of time for intact CSG, ZnSG and CZnSG coatings immersed in 0.86 M NaCl for 24 hours.

Figure 6. Bode and Nyquist plots produced using data obtained during EIS investigations of a.) CSG and b.) CZnSG coatings immersed in 5 % NaCl for 24 hours. The input AC amplitude was 10 mV and the frequency range was from 0.05 Hz to 100 kHz.

Figure 7. SVET derived surface maps showing the distribution of normal current density j_z above intact a.) CSG, b.) ZnSG and c.) CZnSG samples freely corroding in near neutral 0.86 M NaCl after various immersion times.

Figure 8. SVET derived a.) integrated anodic current density and b.) accumulated mass loss as a function of time in the case of intact CSG, ZnSG and CZnSG coatings immersed in 0.86 M NaCl for 24 hours.

Figure 9. SVET derived normal current density values measured above CSG, ZnSG and CZnSG coatings in the presence of a 5 mm x 2 mm (12 % of total area) defect after various times of immersion in 0.86 M NaCl. The optical images show the surface appearance of each sample following immersion in 0.86 M NaCl for 24 hours.

Figure 10. A plot of the j_z values recorded along a.) the dotted lines shown in Figure 9 after various immersion times shown along with schematics showing the mechanism by which coatings are believed to provide sacrificial protection to the steel substrate at coating defects.

Figure 11. SVET derived a.) integrated anodic current density and b.) accumulated mass loss as a function of time in the case that 5 mm x 2 mm (12 % total area) artificial defect is created in the CSG, ZnSG and CZnSG coatings which are then immersed in 0.86 M NaCl for 24 hours.

Figure 12. SVET derived normal current density values measured above ZnSG coatings in the presence of a a.) 5 mm x 2 mm (12 % of total area), b.) 5 mm x 4 mm (26 % of

total area), c.) 7 mm x 6 mm (52% of total area) defect after various times of immersion in 0.86 M NaCl.

Figure 13. SVET derived a.) integrated anodic current density and b.) accumulated mass loss as a function of time in the case that artificial defects of varying size are created in ZnSG coatings which are then immersed in 5 % NaCl for 24 hours.

9. References

1. M. Guglielmi, Journal of Sol–Gel Science and Technology. **8**, 443 (1997).
2. D. Wang, G. P. Bierwagen, Progress in Organic Coatings. **64**, 327 (2009).
3. D. Balgude, A. Sabnis, Journal of Sol-Gel Science and Technology. **64**, 124 (2012).
4. R. Kasemann, H. Schmidt, New Journal of Chemistry. **18** 1117 (1994).
5. M. Fedel, F. Deflorian, S. Rossi, in *Green corrosion chemistry and engineering: opportunities and challenges*, 1st ed, S. K. Sharma, Editor, p. 181, Weinheim: Wiley-VCH Verlag GmBH & Co. (2012).
6. J. Kron, K. J. Deichmann, K. Rose, in *Self-Healing Properties of New Surface Treatments (EFC 58)*, L. Fedrizzi, W. Fürbeth, F. Montemor, Eds., p.105, Leeds: Institute of Materials, Minerals and Mining (2011).
7. Y-S. Li, W. Lu, Y. Wang, T. Tran, Spectrochima Acta A. **73**, 922 (2009).
8. L. K. Tan, A. M. Soutar, Thin Solid Films. **516**, 5706 (2008).
9. Z. Feng, Y. Liu, G. E. Thompson, P. Skeldon, Electrochima Acta. **55**, 3518 (2010).
10. A.L.K. Tan, A. M. Soutar, I. F. Annergren, Y. N. Liu, Surface and Coatings Technology. **198**, 478 (2005).
11. N. Norzita, M. Haziq, M. Zurina, International Journal of Chemical and Environmental Engineering. **3**, 267 (2012).
12. G. Parashar, D. Srivastava, R. Kumar, Progress in Organic Coatings. **42**, 1 (2001).
13. P. Zarras, J. D. Stenger-Smith, in *Intelligent Coatings for Corrosion Control*, A. Tiwari, J. Rawlins, L. H. Hihara, Eds., p. 59, Butterworth Heinemann (2015).
14. T. L. Metroke, R. L. Parkhill, E. T. Knobbe, Progress in Organic Coatings. **41**, 233 (2001).
15. R. B. Figueira, C. J. R. Silva, E. V. Pereira, Surface and Coatings Technology. **265**, 191 (2015).

16. C. A. Sáenz, E. Martin-Ugarte, J. B. Jorcin, G. Imbuluzqueta, P. S. Coloma, U. Izagirre-Etxeberria, Journal of Sol-Gel Science and Technology. **89**, 264 (2019).

17. P. Savignac, M. J. Menu, M. Gressier, B. Denat, Y. El Khadir, S. Manov, F. Ansart, Molecules. **23**, 1079 (2018).

18. C. M. Abreu, M. Izquierdo, P. Merino, X. R. Novoa C. Perez, Corrosion. **55**, 1173 (1999).

19. R. Barajas, M. Morcillo, J.M. Bastidas, S. Feliú, Pinturas y Acabados. **33**, 55 (1991).

20. . S. Feliú, R. Barajas, J.M. Bastidas, M. Morcillo, Journal of Coatings Technology. **61**, 63 (1989).

21. R. A. Armas, C. A. Gervasi, A. Disarli, S. G. Real, J. R. Vilche, Corrosion. **48** (5), 379 (1992).

22. F. Theiler, Corrosion Science. **14**, 405 (1974).

23. D. Pereira, J. Scantlebury, M. Ferreira, M. Almeida, Corrosion Science. **30**, 1135 (1990).

24. S. Lindquist, L. Meszaros, L. Svenson, Journal of the Oil and Colour Chemists' Association. **68**, 10 (1985).

25. R. Fernandez-Prini, S. Kapusta, Journal of the Oil and Colour Chemists' Association. **62**, 93 (1979).

26. O. O. Knudsen, U. Steinsmo, M. Bjordal, Progress in Organic Coatings. **54**, 224 (2005).

27. H. Marchebois, M. Keddam, C. Savall, J. Bernard, S. Touzain, Electrochimica Acta. **49**, 1719 (2004).

28. M. Morcillo, R. Barajas, S. Feliu, J. M. Bastidas, Journal of Materials Science. **25**, 2441 (1990).

29. J. E. O. Mayne, U. R. Evans, Soc. Chem. Ind. Rev. **22**, 109 (1944).

30. J. E. O. Mayne, Soc. Chem. Ind. Rev. **66**, 93 (1947).

31. T. K. Ross, J. Wolstenholme, Corrosion Science. **17**, 341 (1977).

32. S. E. Faidi, J. D. Scantlebury, P. Bullivant, N. T. Whittle, R. Savin, Corrosion Science. **35**, 1319 (1993).

33. M. Yekehtaz, C. Klesen, S. Benfer, W. Bleck, W. Fürbeth, Materials and Corrosion. **63**, 940 (2012).

34. O. Razavizadeh, M. Ghorbani, Journal of Sol-Gel Science and Technology. 79 (2016) 133.

35. B. Kannan, C. F. Glover, H. N. McMurray, G. Williams, J. R. Scully, Journal of the Electrochemical Society. **165**, C27 (2018).

36. L.Y.L. Wu, E. Chwa, Z. Chen, X.T. Zeng, Thin Solid Films. 516, 1056 (2008).

37. ISO 8501-1: 2007. Preparation of steel substrates before application of paints and related products- Visual assessment of surface cleanliness- Part 1: Rust grades and preparation grades of uncoated steel substrates and of steel substrates after overall removal of previous coatings. Geneva, ISO Copyright Office (2007).

38. G. Löbbert, in *Ullmann's Encyclopedia of Industrial Chemistry (Vol. 27)*, F. Ullman, Ed., p. 181-213, Wiley-VCH (2011).

39. C.A. Gervasi, A.R. Di Sarli, E. Cavalcanti, O. Ferraz, E.C. Bucharsky, S.G. Real, J.R. Vilche, Corrosion Science. **36**, 1963 (1994)

40. ASTM D3359-17, Standard Test Methods for Rating Adhesion by Tape Test, ASTM International, West Conshohocken, PA (2017).

41. ISO 14993:2001. Corrosion of metals and alloys - Accelerated testing involving cyclic exposure to salt mist, "dry" and "wet" conditions. Geneva, ISO Copyright Office (2001).

42. G. Williams, H. N. McMurray, J. Electrochem. Soc., **155**, C340 (2008).

43. S. Bohm, H. N. McMurray, S. M. Powell, D. A. Worsley, Electrochmica Acta, 45, **2165** (2000).

44. D. Worsley, H. N. McMurray, A. Belghazi, Chem. Commun., **24**, 2369 (1997).

45. S. M. Powell, D. A. Worsley, British Corrosion Journal, **36**, 42 (2001).

46. G. Williams, H. N. McMurray, R. Grace, Electrochimica Acta, **55**, 7824 (2010).

47. H. S. Isaacs, G. Kissel, J. Electrochem. Soc. **119**, 1628 (1972).

48. H. S. Isaacs, J. Electrochem. Soc., **138**, 722 (1991).

49. BS EN 15112:2006

50. National Association of Corrosion Engineers SP0169-2013

51. National Association of Corrosion Engineers SP 05 75- 2007

52. National Association of Corrosion Engineers SP0176-2007

53. H. N. McMurray, D. Williams, D. A. Worsley, Journal of the Electrochemical Society. **150**, B567 (2003)

54. A. C. Bastos, M. C. Quevedo, M. G. S. Ferreira, Corrosion Science. **92**, 309 (2015).

55. T. Lutzler, T.V.J. Charpentier, R. Barker, S. Soltanahmadi, W. Taleb, C. Wang, A. Alejo-Rodriguez, E. Perre, H. Schneider, A. Neville, Materials Chemistry and Physics. **216,** 272 (2018).

56. L. Claire, G. Marie, G. Julien, S. Jean-Michel, R. Jean, M. Marie-Joëlle, R. Stefano, F. Michele, Progress in Organic Coatings. **99**, 337 (2016).

57. L. Vivar Mora, S. Naik, S. Paul, R. Dawson, A. Neville, R. Barker, Surface and Coatings Technology. **324**, 386 (2017).

58. G. P. Bierwagen, L. Hi, J. Li, L. Ellingson, D. E. Tallman, Progress in Organic Coatings. **39**, 67 (2000).

59. R. A. Serway, J. S. Faughn. *College Physics*. 6th edition. P. 519 Canada: Thomson Learning (2003).

60. G. Chandrashekhar, M. Shafer, MRS Proceedings. **73** (1986) 705.

61. H. N. McMurray, S. R. Magill, B. D. Jeffs, Ironmaking and Steelmaking. **23**, 183 (1996).

62. H. N. McMurray, D. A. Worsley, in *Research in Chemical Kinetics Vol. 4*, R. G. Compton, G. Hancock, Eds., p.149, Blackwell Science, Oxford UK (1997).

63. N. Wint, K. Khan, J. H. Sullivan, H. N. McMurray, Journal of The Electrochemical Society, **166**, C3028 (2019).

64. N. Wint, N. Cooze, J. R. Searle, J. H. Sullivan, G. Williams, H. N. McMurray, G. Luckeneder, C. Riener, Journal of the Electrochemical Society, **166**, C3147 (2019).

65. K. Ogle, V. Baudu, L. Garrigues, X. Philippe, Journal of the Electrochemical Society. **147**, 3654 (2000).

66. K. Ogle, S. Morel, D. Jacquet, Journal of the Electrochemical Society. **153**, B1 (2006).

67. R. Krieg, M. Rohwerder, S. Evers, B. Schuhmacher, J. Schauer-Pass, Corrosion Science. **65**, 119 (2012).

68. F. Thébault, B. Vuillemin, R. Oltra, K. Ogle, C. Allély, Electrochimica Acta. **53** (2008) 5226.

69. F. Thébault, B. Vuillemin, R. Oltra, C. Allély, K. Ogle, Electrochimica Acta. **56** (2011) 8347.

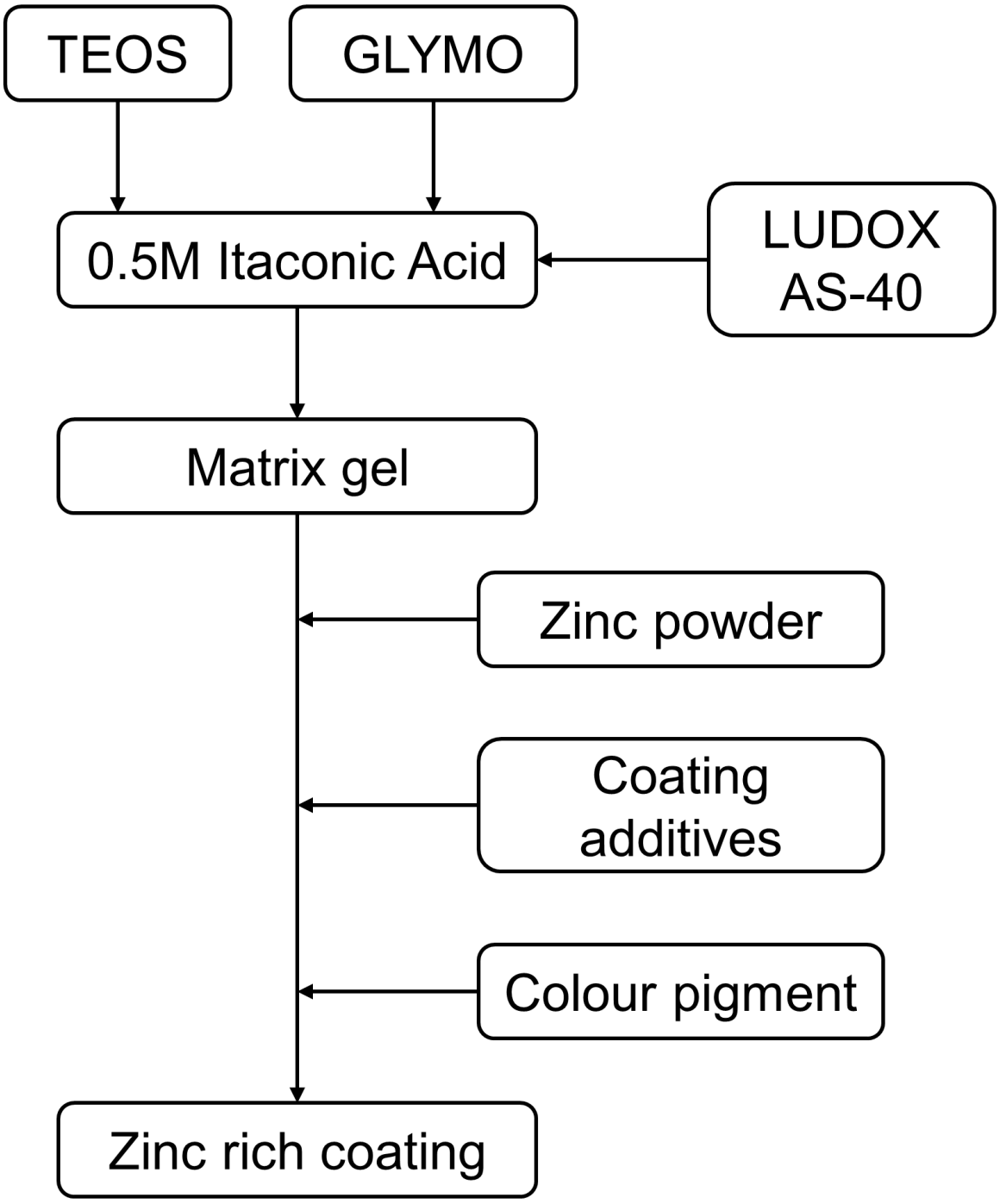
TEOS
GLYMO
0.5M Itaconic Acid
LUDOX AS-40
Matrix gel
Zinc powder
Coating additives
Colour pigment
Zinc rich coating

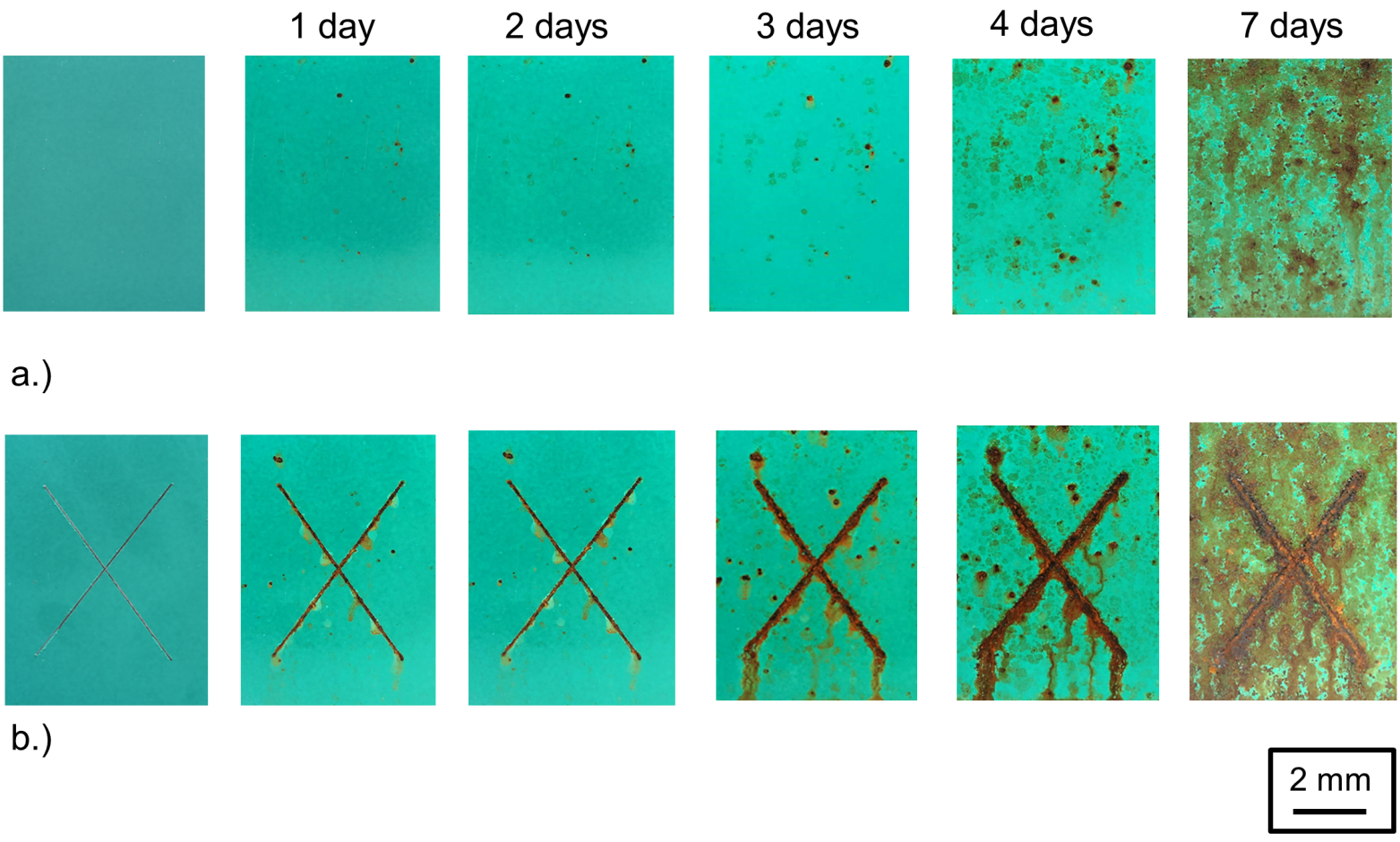
1 day
2 days
3 days
4 days
7 days
a.)
b.)
2 mm

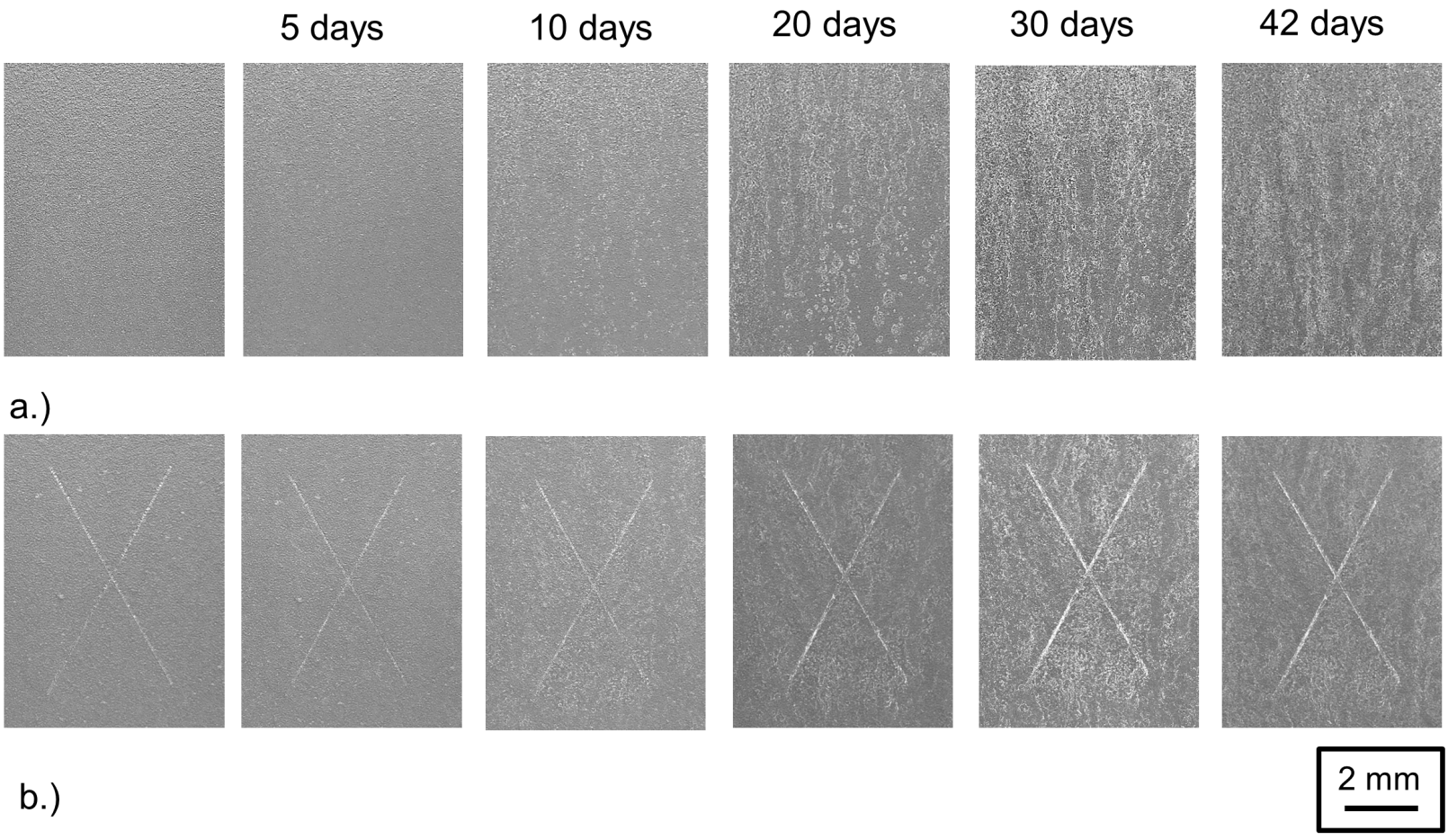
5 days
10 days
20 days
30 days
42 days
a.)
b.)
2 mm

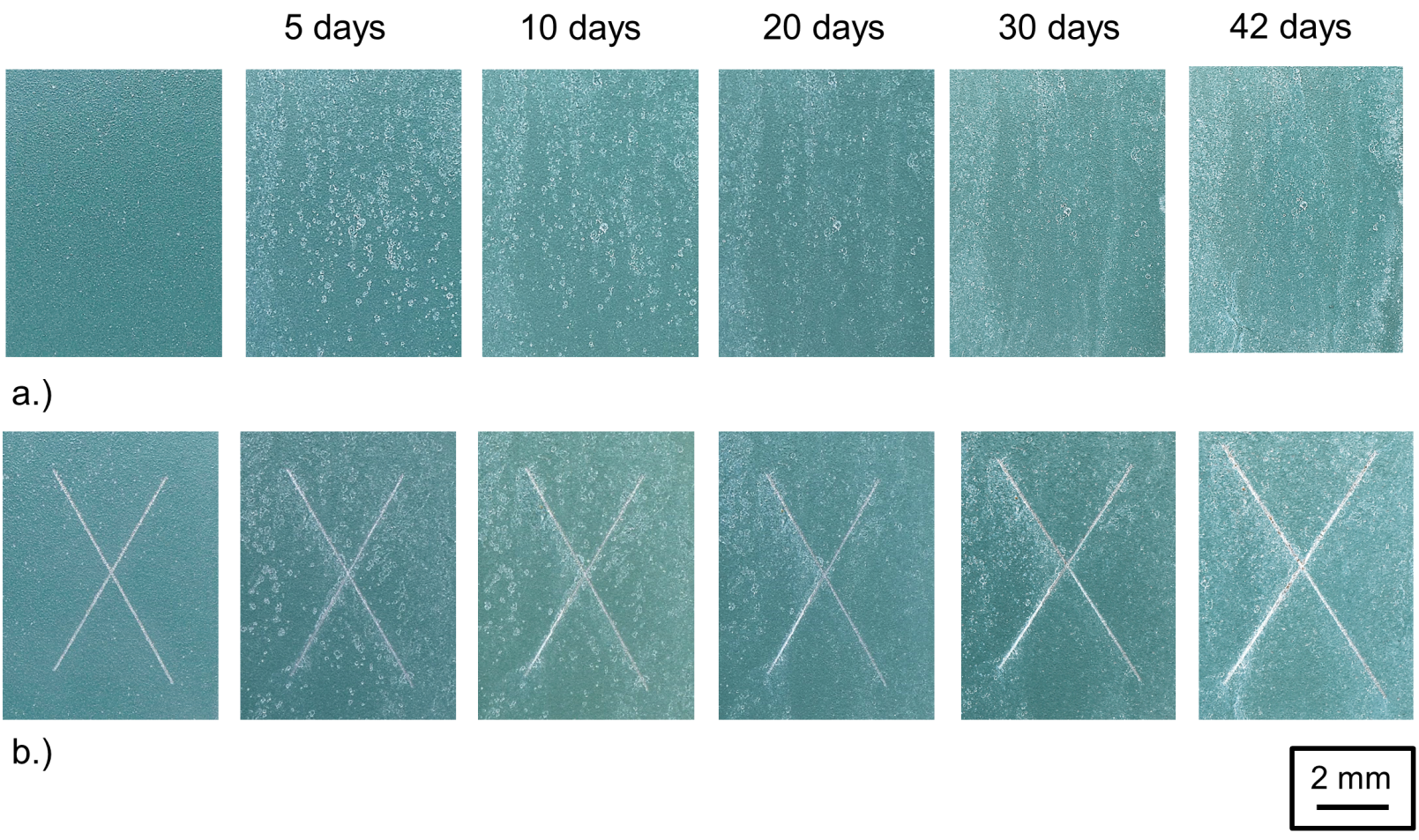
5 days
10 days
20 days
30 days
42 days
a.)
b.)
2 mm

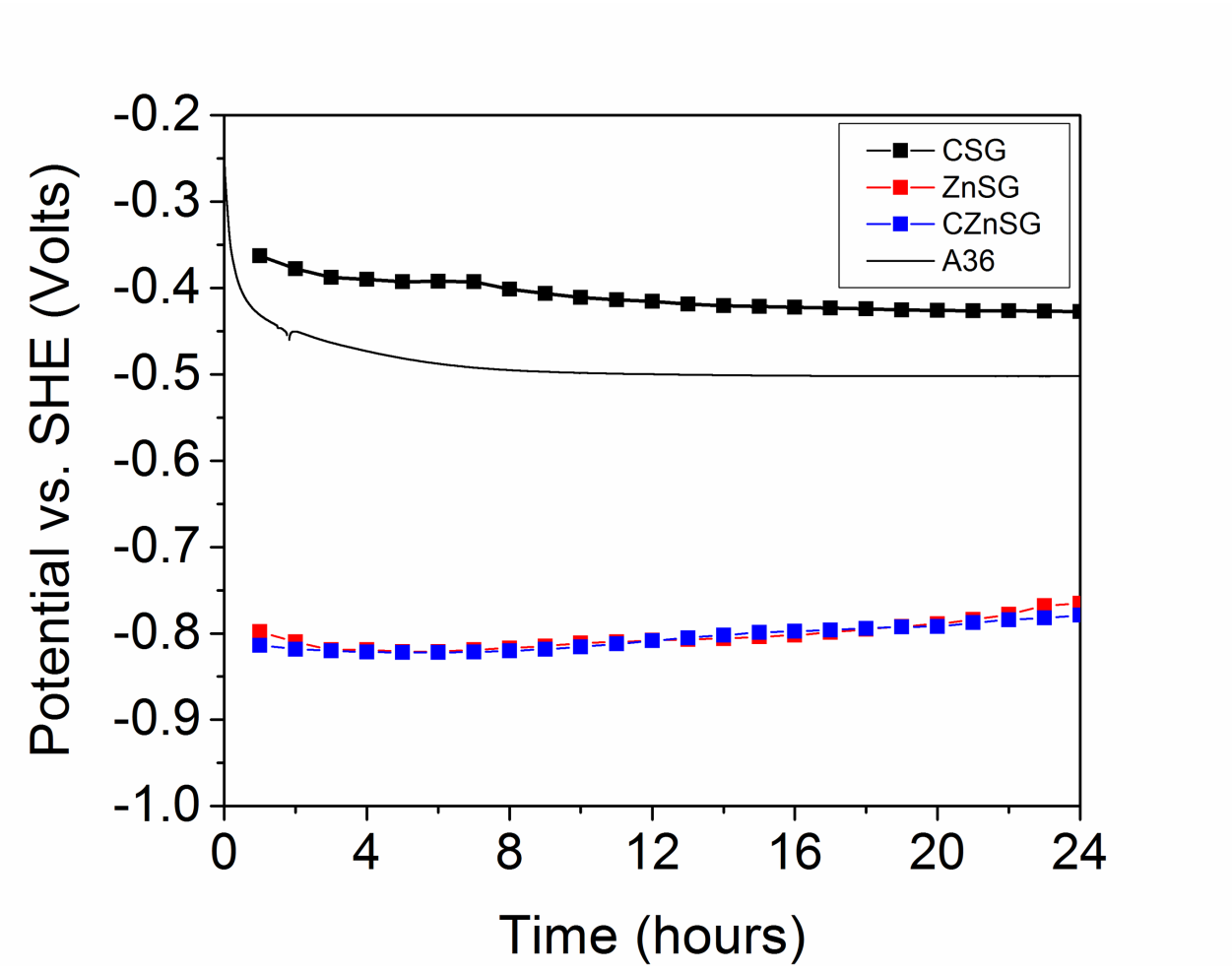
Potential vs. SHE (Volts)
-0.2
-0.3
-0.4
-0.5
-0.6
-0.7
-0.8
-0.9
-1.0
0
4
8
12
16
20
24
Time (hours)
CSG
ZnSG
CZnSG
A36

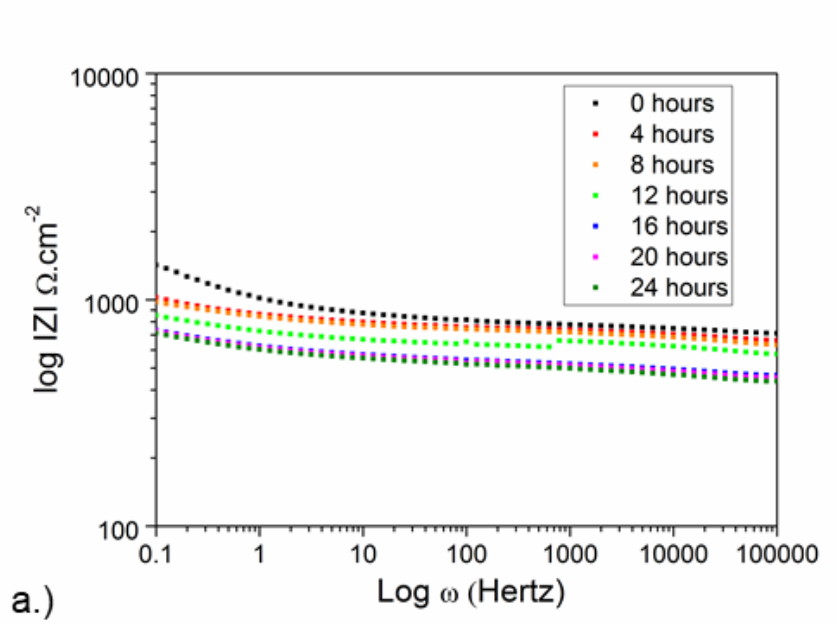
10000
1000
100
log IZI Ω.cm-2
0.1
1
10
100
1000
10000
100000
Log ω (Hertz)
0 hours
4 hours
8 hours
12 hours
16 hours
20 hours
24 hours

a.)

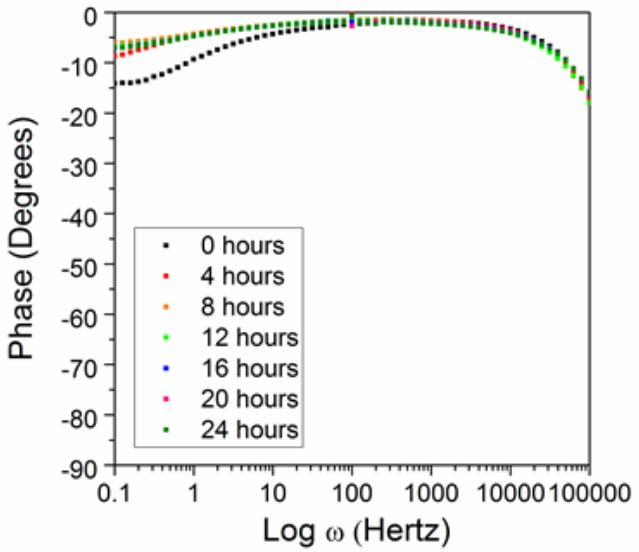
0
-10
-20
-30
-40
-50
-60
-70
-80
-90
Phase (Degrees)
0.1
1
10
100
1000
10000
100000
Log ω (Hertz)
0 hours
4 hours
8 hours
12 hours
16 hours
20 hours
24 hours

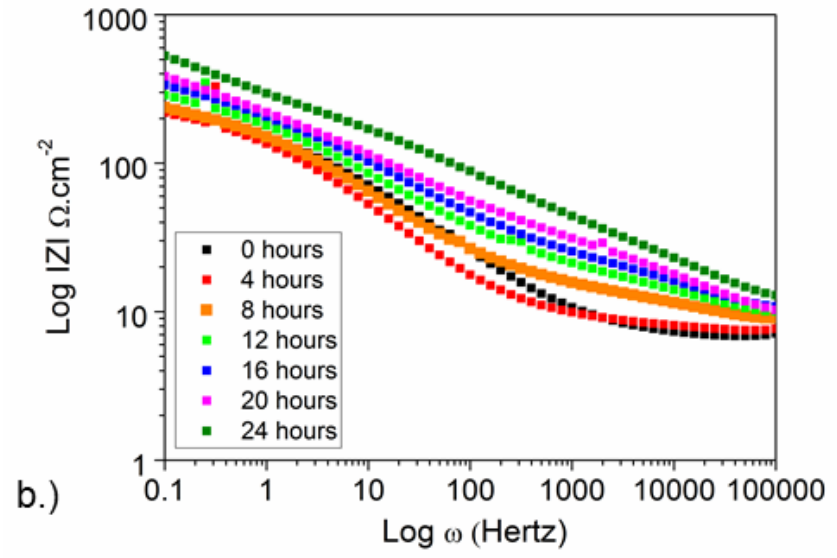
1000
100
10
1
Log IZI Ω.cm-2
0.1
1
10
100
1000
10000
100000
Log ω (Hertz)
0 hours
4 hours
8 hours
12 hours
16 hours
20 hours
24 hours

b.)

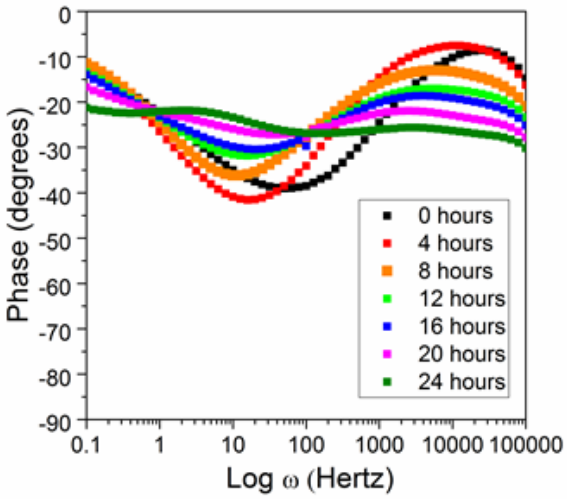
0
-10
-20
-30
-40
-50
-60
-70
-80
-90
Phase (degrees)
0.1
1
10
100
1000
10000
100000
Log ω (Hertz)
0 hours
4 hours
8 hours
12 hours
16 hours
20 hours
24 hours

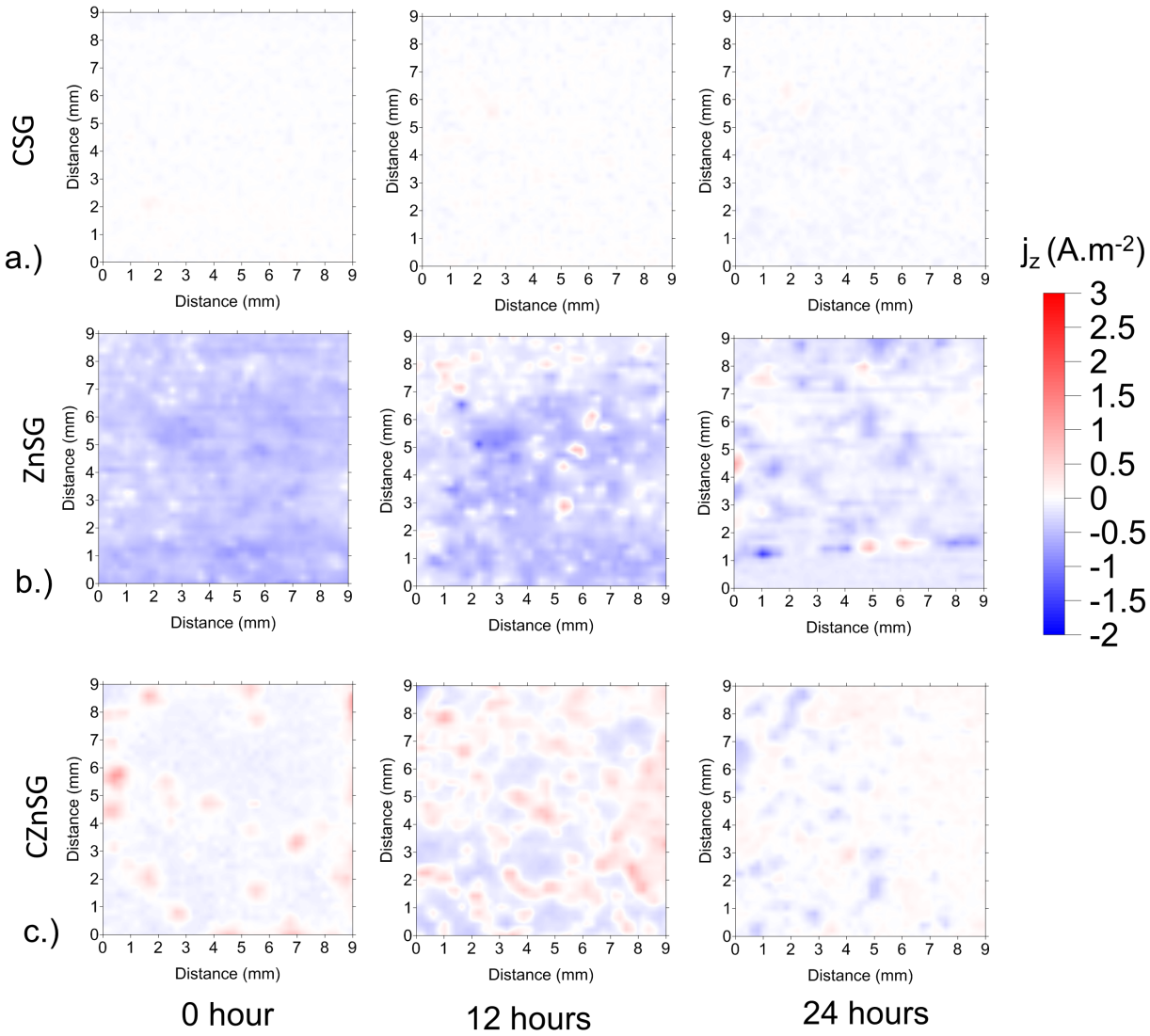
CSG
a.)
ZnSG
b.)
CZnSG
c.)
Distance (mm)
Distance (mm)
0 hour
12 hours
24 hours
j_z (A.m^{-2})
3
2.5
2
1.5
1
0.5
0
-0.5
-1
-1.5
-2

a.)

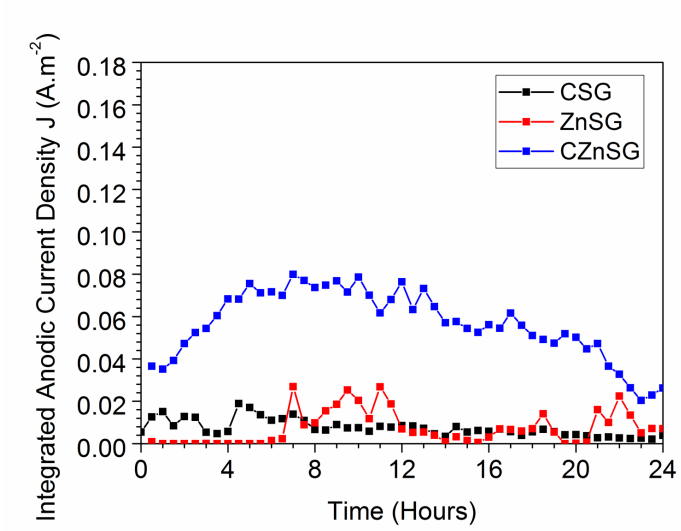
Integrated Anodic Current Density J (A.m-2)
0.18
0.16
0.14
0.12
0.10
0.08
0.06
0.04
0.02
0.00
0
4
8
12
16
20
24
Time (Hours)
CSG
ZnSG
CZnSG

b.)

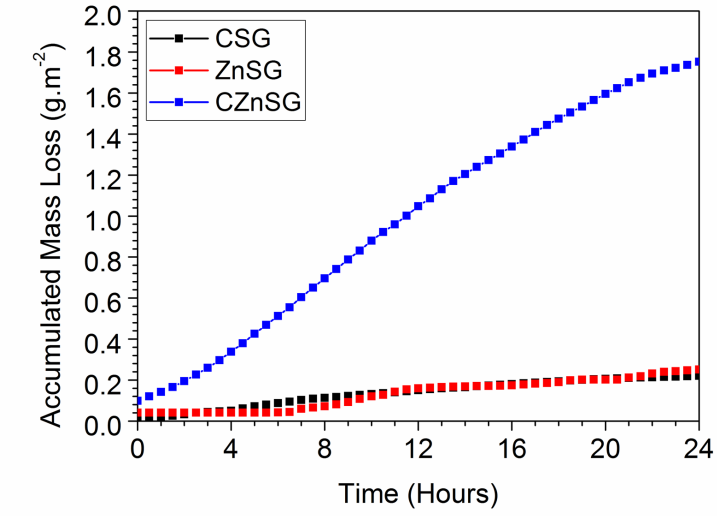
Accumulated Mass Loss (g.m-2)
2.0
1.8
1.6
1.4
1.2
1.0
0.8
0.6
0.4
0.2
0.0
0
4
8
12
16
20
24
Time (Hours)
CSG
ZnSG
CZnSG

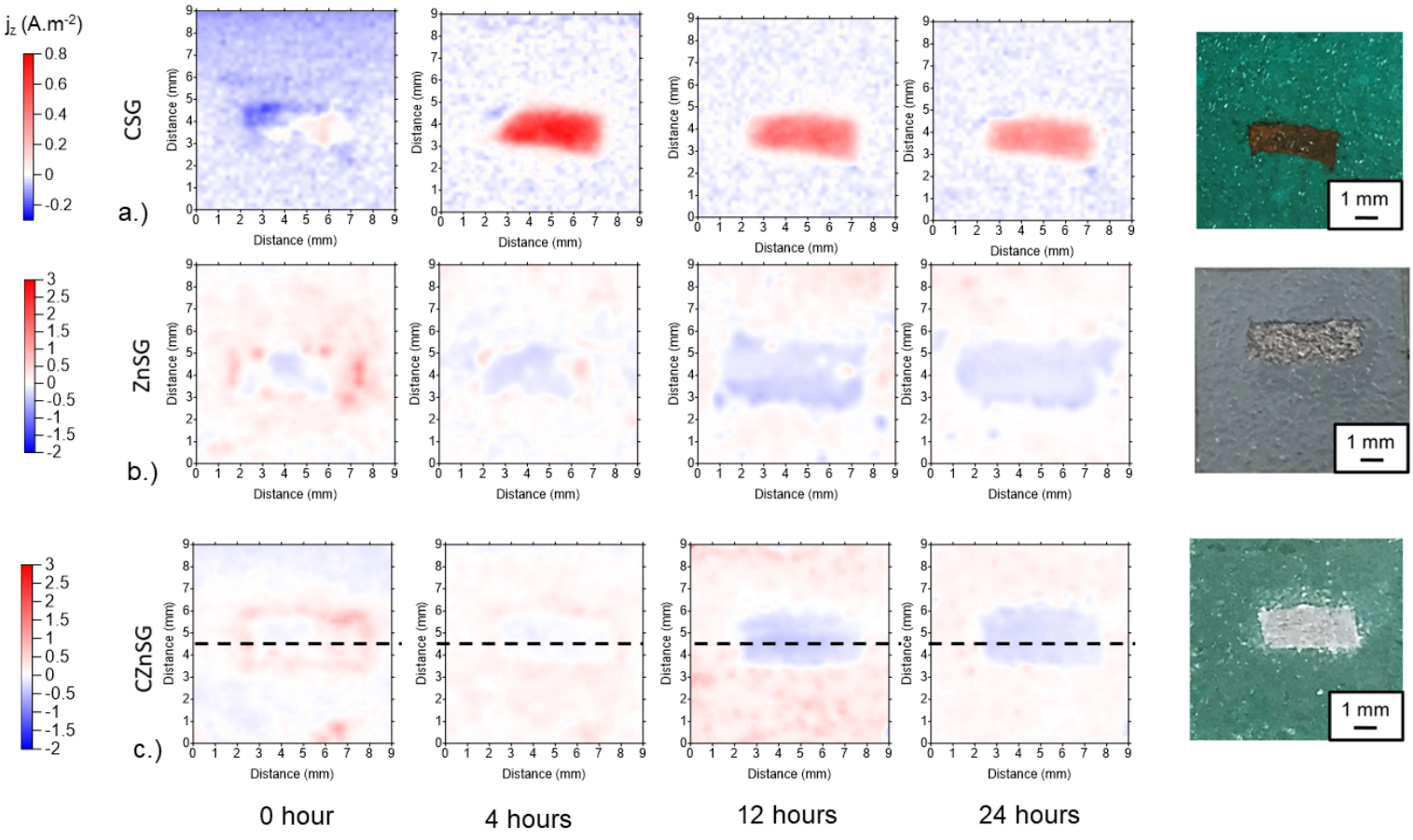
j_z (A.m^{-2})
0.8
0.6
0.4
0.2
0
-0.2
CSG
a.)
3
2.5
2
1.5
1
0.5
0
-0.5
-1
-1.5
-2
ZnSG
b.)
CZnSG
c.)
Distance (mm)
1 mm
0 hour
4 hours
12 hours
24 hours

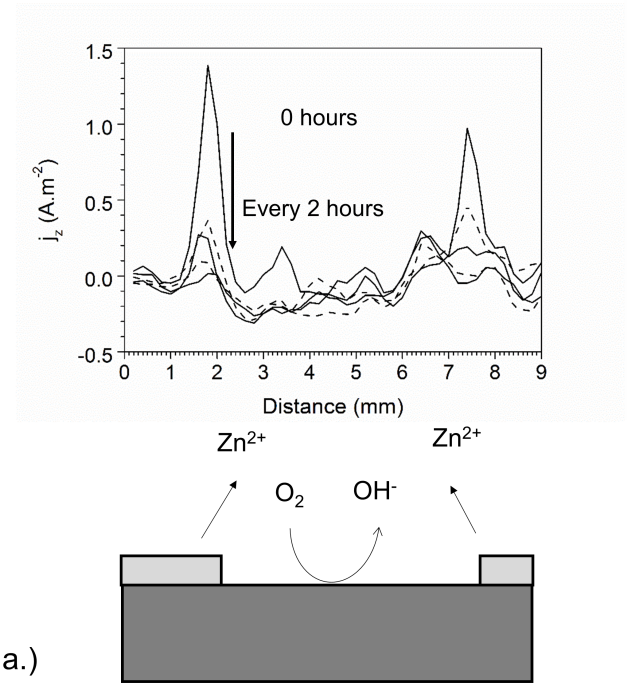
1.5
1.0
0.5
0.0
-0.5
0 hours
Every 2 hours
j_z (A.m^{-2})
0 1 2 3 4 5 6 7 8 9
Distance (mm)
Zn^{2+}
Zn^{2+}
O_2
OH^-

a.)

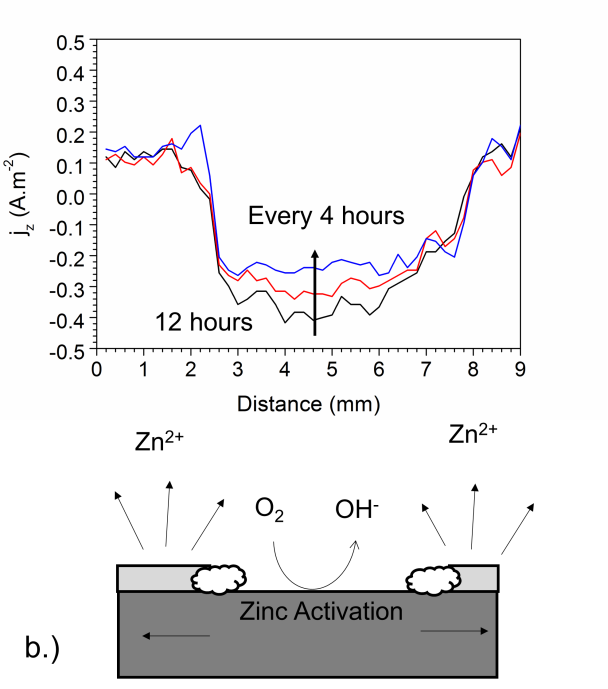
0.5
0.4
0.3
0.2
0.1
0.0
-0.1
-0.2
-0.3
-0.4
-0.5
Every 4 hours
12 hours
j_z (A.m^{-2})
0 1 2 3 4 5 6 7 8 9
Distance (mm)
Zn^{2+}
Zn^{2+}
O_2
OH^-
Zinc Activation

b.)

a.)

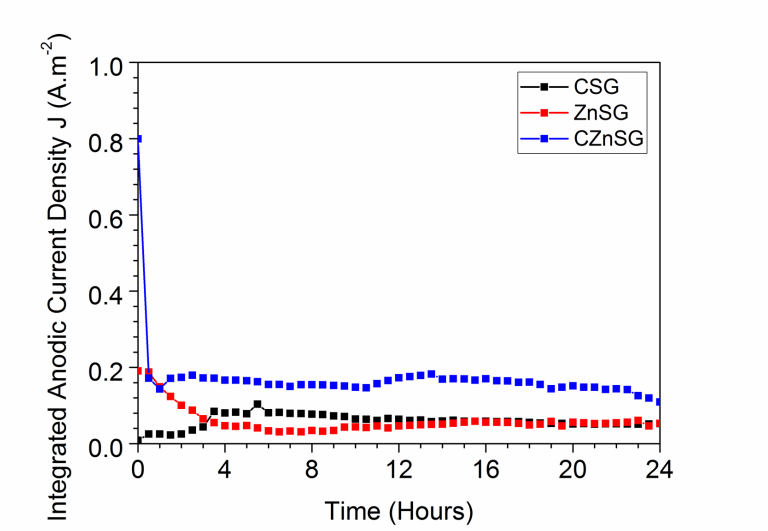
Integrated Anodic Current Density J (A.m-2)
1.0
0.8
0.6
0.4
0.2
0.0
0
4
8
12
16
20
24
Time (Hours)
CSG
ZnSG
CZnSG

b.)

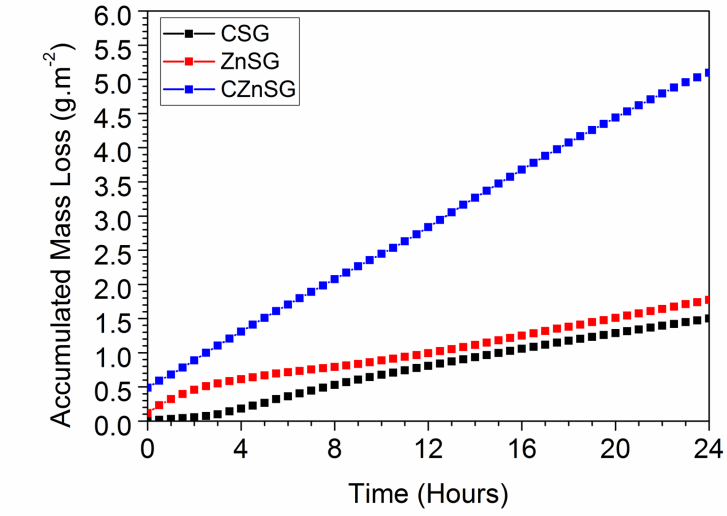
Accumulated Mass Loss (g.m-2)
6.0
5.5
5.0
4.5
4.0
3.5
3.0
2.5
2.0
1.5
1.0
0.5
0.0
0
4
8
12
16
20
24
Time (Hours)
CSG
ZnSG
CZnSG

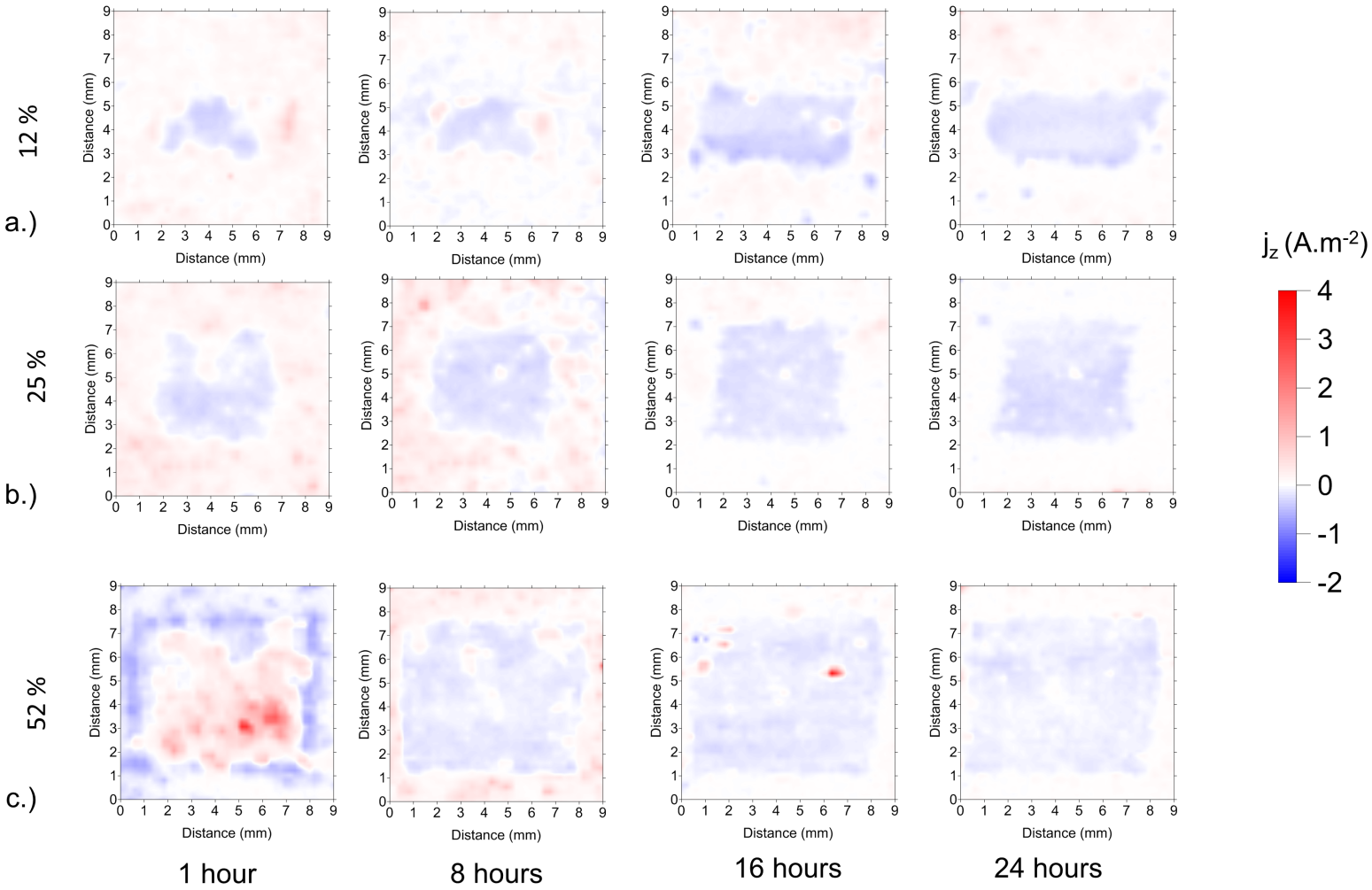
a.)
12 %
b.)
25 %
c.)
52 %
Distance (mm)
1 hour
8 hours
16 hours
24 hours
j_z (A.m^{-2})
4
3
2
1
0
-1
-2

a.)

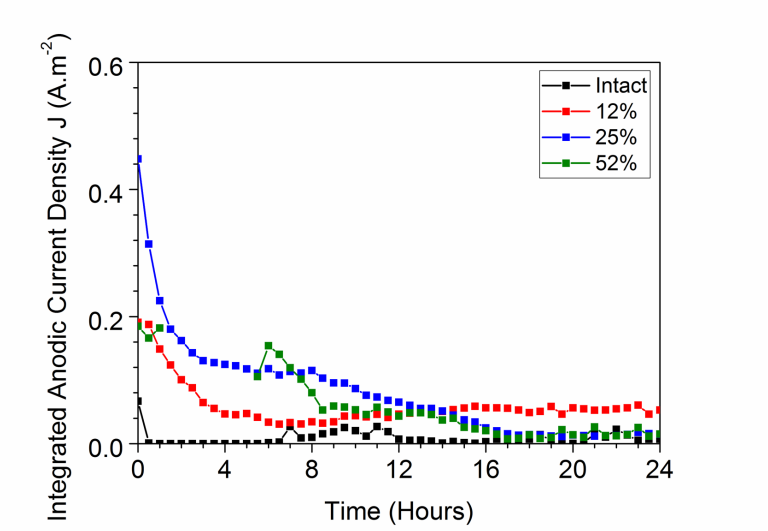
Integrated Anodic Current Density J (A.m-2)
0.6
0.4
0.2
0.0
0
4
8
12
16
20
24
Time (Hours)
Intact
12%
25%
52%

b.)

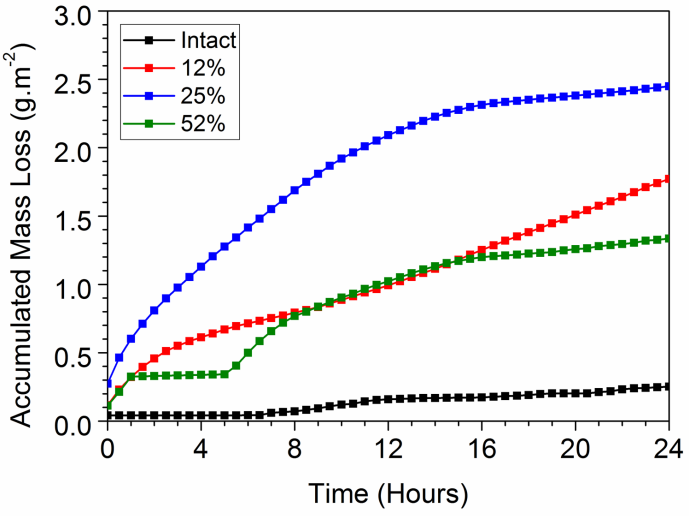
Accumulated Mass Loss (g.m-2)
3.0
2.5
2.0
1.5
1.0
0.5
0.0
0
4
8
12
16
20
24
Time (Hours)
Intact
12%
25%
52%